This is the accepted manuscript of the following article: Fernández-Ramos, A., Siebrand, W., & Smedarchina, Z. (2013). New interpretation of proton and deuteron tunneling in 2'-methylacetophenone. Chemical Physics Letters, 586, 61-66. doi: 10.1016/j.cplett.2013.09.020

© 2013 Elsevier B.V. This manuscript version is made available under the CC-BY-NC-ND 4.0 license (http://creativecommons.org/licenses/by-nc-nd/4.0/)

Graphical Abstract (pictogram) (for review)

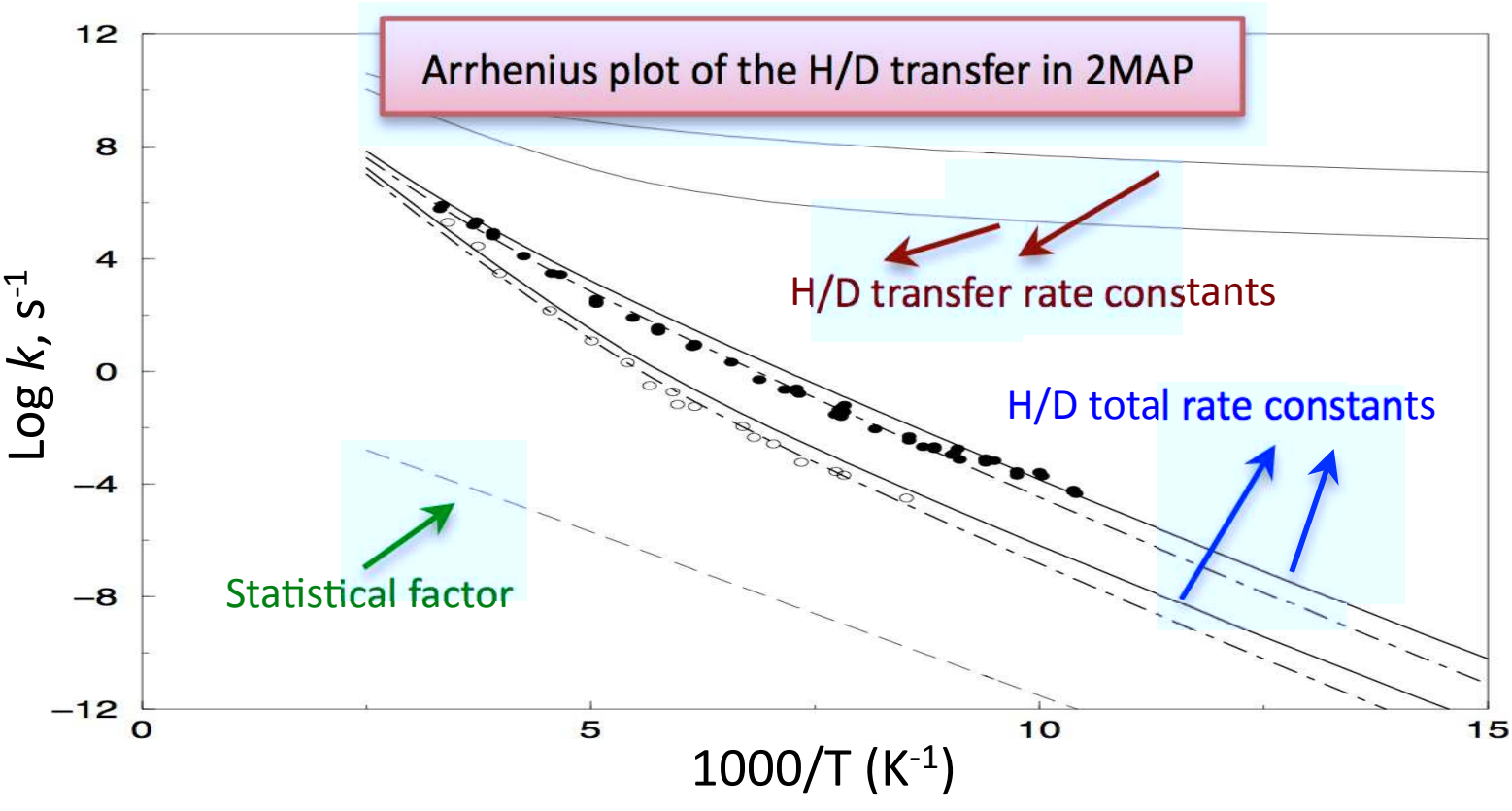

*The Manuscript
Click here to view linked References

New interpretation of proton and deuteron tunneling in 2'-methylacetophenone

Antonio Fernández-Ramos,[a] Willem Siebrand,[b] and Zorka Smedarchina[a,b]

July 17, 2013

[a]Department of Physical Chemistry, Faculty of Chemistry and
Centro Singular de Investigación en Química Biolóxica e Materiales Moleculares (CIQUS)
University of Santiago de Compostela, 15706 Santiago de Compostela, Spain
[b] National Research Council of Canada, Ottawa, K1A 0R6 Canada

Abstract

The enol–keto transition rate constants in 2'-methylacetophenone observed by Grellmann et al. [Chem. Phys. Lett. 95 (1983) 195] are calculated from first principles. The results reinterpret the proposed mechanism and show that proton tunneling is preceded by dissociation of a substrate-solvent complex rather than by rotamer interconversion.

1 Introduction

Although proton tunneling is a well-established mechanism in chemical kinetics in general and enzyme kinetics in particular, there are few experimental and theoretical studies in which this transfer process has been followed over a wide range of temperatures for both protons and deuterons. Experimentally, such a study requires measurement of rate constants that vary greatly, often over many orders of magnitude; theoretically, it requires many time-

consuming calculations based on methods that can deal accurately with both overbarrier and throughbarrier transfer mechanisms. The temperature dependence of the transfer rate constants will typically give rise to a curved Arrhenius plot, i.e. a nonlinear relationship between the logarithm of the rate constant and the inverse temperature. Although this is well understood, the quasi-linearity of such plots when the measurements are confined to a narrow temperature interval has prevented proper exploitation of this curvature. While the parameters derived from such quasi-linear plots have been recognized as evidence for tunneling, they have rarely been used to investigate the physical parameters governing the tunneling process [1].

The search for a molecule that exhibits a curved Arrhenius plot along with a strong kinetic isotope effect (KIE, defined as the ratio of H and D transfer rate constants) and is small enough to allow high-level calculations of these rate constants led us to the enol–keto transition in 2'-methylacetophenone (2MAP). This is an historically important example of a tunneling system, studied experimentally by Scaiano [2] and, in much greater detail, by Grellmann, Weller and Tauer (GWT) [3]; the latter study covers a wide range of temperatures for both H and D transfer and presents a semi-empirical analysis of the transfer mechanism. Optical excitation turns the ketone into a mixture of two enol isomers, labeled **Z** and **E** by the authors, of which only one, namely **Z**, was found to reketonize within the timeframe of the experiment, the difference being due to the orientation of the $=C(CH_3)OH$ side chain relative to the $=CH_2$ group. The **Z** isomer occurs in the form of two rotamers, with different orientations of the OH bond relative to this group, as depicted in Fig. 1; GWT assumed the rotamer with the orientation away from this group, labeled **Z-I**, to be planar and the one with the orientation towards the group, labeled **Z-II**, to be nonplanar because of H-H repulsion. The two rotamers interconvert by rotation about the CO bond. GWT measured the first-order rate of decay of **Z** by monitoring the decay of the enol absorption band at 410 nm following flash excitation of the ketone. They found that this rate exhibits a strong temperature dependence in the range 118-298 K as well as a KIE that increased rapidly with decreasing temperature, indicating that the enol–keto transition involves proton tunneling. After carrying out semi-empirical tunneling calculations based on transfer through a symmetric Eckart barrier, they concluded that the observed activation energy was far too

large to derive solely from the tunneling process.

To interpret the observed rate constants, they therefore ascribed them to two consecutive processes, namely interconversion between the two **Z** rotamers followed by proton transfer from the hydroxyl to the methylene group. To be able to assign part of the observed activation energy to interconversion, they had to assume that the rotamer with the shorter transfer distance, i.e. rotamer **Z-II** in Fig. 1, has a higher energy than rotamer **Z-I**. To account for the observed exponential decay signals, they further assumed rotamer interconversion to be much faster than tunneling transfer and represented it by an equilibrium constant, which they described by a weighted Boltzmann factor $C\ \exp[-(E_{\mathrm{II}} - E_{\mathrm{I}})/k_B T]$, where C is a statistical factor. Strictly speaking C should be represented by the ratio of the partition functions of the two rotamers, but in the absence of a vibrational force field it seems reasonable to approximate it by a factor of 2, since there should be two forms of the nonplanar rotamer **Z-II**, but only one of **Z-I** if it is planar. However, GWT used a value $C = 10$, which is clearly unjustified, since the principle of microscopic reversibility implies that the forward and back transitions proceed by the same route. The removal of a factor of five from the calculated transition rate constants implies that the deduced values for the proton transfer distance and the two activation barriers require revision.

However, there is another, more serious reason to revisit the interpretation, namely the fact that it does not take account of the presence of alcohol in the solvent. Since enols are acidic, they are proton donors and tend to form strong hydrogen bonds with proton acceptors. This is well known from analogous reactions involving phenols [4]. Such hydrogen bonding would reduce tunneling because it introduces an equilibrium constant between free and hydrogen-bonded enol groups. Hence the assumption that rotamer interconversion but not hydrogen bonding with the solvent affects the proton transfer rate needs to be reconsidered. Since both processes would contribute a Boltzmann factor to the rate, they would be kinetically indistinguishable. To decide whether either or both of them contribute to the observed rate constants, we need a quantitative evaluation of the energetics of the system. This is also required for the replacement of the empirical symmetrical Eckart barrier by a calculated multidimensional potential-energy surface that includes the strong asymmetry of the barrier as well as all vibrational degrees of freedom.

Since the mechanism proposed by GWT hinges on the relative energies of the two enol rotamers **Z-I** and **Z-II**, we first calculate the structure and energy of their equilibrium configurations and relevant transition states for the unsolvated molecule. These results we use as input in the approximate instanton method (AIM) as implemented in the DOIT1.2 program [5], which is particularly well suited to calculate rate constants for proton and deuteron transfer over a wide range of temperatures, since it does not require evaluation of the tunneling trajectories. We then calculate the structure and energy of the relevant configurations of the hydrogen-bonded complexes and compare the calculated rate constants with experimental values so as to be able to draw conclusions about the transfer mechanism.

2 The unsolvated molecule

To investigate proton transfer in the isolated 2MAP molecule, we focus on five stationary structures, namely **Z-I**, **Z-II**, the keto form, and the transition states between the two rotamers and between **Z-II** and the keto form. For this purpose we perform MPWB1K/6-31+G(d,p) [6] electronic calculations using Gaussian03 [7].

The structure and energy of **Z-I**, **Z-II**, and the keto form are illustrated in Fig. 1 and Table 1. It follows immediately that the energy of the **Z-I** rotamer exceeds that of the **Z-II** rotamer by almost 4 kcal/mol, so that the mechanism proposed by GWT does not apply. Hence **Z-I** will not be significant for the rate of proton transfer in the isolated molecule. The transition state between **Z-II** and the keto form, also illustrated in Fig. 1, exhibits a very asymmetric barrier corresponding to an exothermicity of 36.64 kcal/mol and a barrier height of 7.28 kcal/mol illustrated in Fig. 2. The experimental data of GWT cover a temperature range between 100 K and 300 K, indicating that the mechanism of proton transfer governed by this potential will change from deep tunneling at the lower limit to thermally-activated transfer at the upper limit. The AIM/DOIT1.2 program to be used for the calculation of the rate constants has yielded satisfactory results in our earlier studies of proton transfer across strongly asymmetric barriers in the 1:1 complexes of 7-azaindole [8] and 3-hydroxyisoquinoline [9] with water. Since the method was described there in detail, we limit ourselves to a summary of the approach in the Appendix and concentrate here on

its application to the problem at hand.

The calculated rate constants of the **Z-II**–keto transformation by H and D transfer, denoted as $k_2(T)$, are listed in Table 2 and displayed as thin solid lines in Fig. 3. Comparison with the observed rate constants, also shown in Fig. 3, shows that the calculation greatly overestimates the rate constants and underestimates their temperature dependence. However, a reasonable fit of the form $k(T) = k_2(T)\exp(-E_a/k_BT)$ is obtained if the calculated rate constants are multiplied by a Boltzmann factor corresponding to an energy E_{a}=5.55 kcal/mol, as shown by the thick lines. Since this value is typical for hydrogen bonding between oxygen centers [4], the reaction step assigned to rotamer interchange by GWT can be plausibly assigned to hydrogen-bond breaking. Hence we extend the calculations to solvated molecules.

3 The solvated molecule

To investigate the effect of solvation, we study complexes of 2MAP hydrogen-bonded to a methanol molecule; for simplicity we use methanol rather than ethanol, as it has been found [2,3] that the kinetic data are the same in this solvent as in the solvent mixture containing ethanol used by GWT. The solvating methanol molecule may itself be part of a chain of methanol molecules, but for the present purpose, we assume that the essential part of the solvation effect is covered by the formation of a hydrogen bond between 2MAP and one solvent molecule. There are two ways in which a methanol molecule can form a hydrogen bond with **Z-II**: It can donate its hydroxyl hydrogen to the oxygen of the enol or it can accept the hydrogen of the enol group at its oxygen atom; we denote these complexes by 2MAP-dMe and 2MAP-aMe, respectively. Using the same method as above, we calculate the structure and energetics of the equilibrium configurations and the transition states of both complexes; the results are displayed in Fig. 4 and Table 1. To make the listed stationary state energies comparable to those of the unsolvated molecule, we have subtracted the energy of an isolated methanol molecule. This yields identical energies for the **Z-I** configurations of the two complexes, namely a value of 8.80 kcal/mol below the **Z-I** configuration of the unsolvated molecule. For the **Z-II** configurations, the corresponding energies are 4.34 kcal/mol for

2MAP-dMe and 5.89 kcal/mol for 2MAP-aMe. As expected on the basis of the relative acidities of enols and alcohols, the structure of fig. 4a, in which methanol is the hydrogen donor, is less stable that that of fig. 4b, in which it is the acceptor, at least in the **Z-II** configuration, which is relevant for tunneling. However, in the **Z-I** configuration these energies are virtually the same, which indicates that steric effects play a role as well.

The results indicate that there are at least three pathways for the enol–keto reaction:
(1) An enol-alcohol complex may dissociate, leading to proton transfer in the unsolvated molecule, as calculated in the preceding section; this involves a Boltzmann factor corresponding to the energy of the broken bond, namely 4.34 kcal/mol for 2MAP-dMe and 5.89 kcal/mol for 2MAP-aMe; to the former the energy difference between these two rotamers, 0.98 kcal/mol, should be added to account for the required transfer between them, the **Z-II** configuration of the former being a minority component in the solution.
(2) Transfer may occur directly in 2MAP-aMe; this involves no significant Boltzmann factor, since the **Z-II** configuration of this complex is the dominant component in the solution.
(3) Transfer may occur directly in 2MAP-dMe; this involves a Boltzmann factor corresponding to an energy of about 1.55(=0.98+0.57) kcal/mol, which reflects the low concentration of the **Z-II** configuration of this complex in the solution.

Evidently, the fit shown in Fig. 3 favors the first option. In terms of the quoted energies (in kcal/mol), we express the temperature dependence of the rate constants in the form

$$k(T) = 2K(T)k_2(T)\{[1-\exp(-0.98/k_BT)]\exp(-5.89/k_BT) + \exp[-(0.98+4.34)/k_BT]\}$$
$$\simeq 2K(T)k_2(T)[\exp(-5.89/k_BT) + \exp(-5.32/k_BT)], \quad (1)$$

where $K(T)$ is the equilibrium constant between **Z-I** and **Z-II** and the coefficient 2 reflects the fact that **Z-II** has two structures (non planar) while **Z-I** has only one.

Fig. 3 illustrates this equation, which is in reasonable agreement with the expression $k(T) = k_2(T)\exp(-5.55/k_BT)$ with the empirical Boltzmann factor used in the figure; it therefore qualifies as a valid interpretation of the observations. Hence we conclude that the actual mechanism of the reaction is breaking of the hydrogen bond between 2MAP and the solvent followed by proton transfer in the unsolvated molecule with no significant involvement of rotamer interconversion.

This begs the question why the second and third options do not contribute significantly to the reaction. Explorative calculations show that tunneling in the 1:1 complexes is accompanied by an extensive reorientation of the the methanol relative to MAP. The corresponding very small Franck-Condon factor reduces the tunneling rate to a value where tunneling is no longer competitive with overbarrier transfer. In the solvent such large displacements may be obstructed, but this would imply coupling to low-frequency bath modes, which would have the same effect. The ensuing proton transfer along the minimum energy path would encounter a barrier considerably larger than the barrier involved in breaking the MAP-methanol bond. Hence the favored transfer mechanism will be breaking this bond followed by proton tunneling in the bare molecule.

Moreover, in the stable 2MAP-aMe complex, the **Z-II** configuration is stabilized by the strong hydrogen bond, leading to a significantly higher tunneling barrier. The actual tunneling process would involve two protons, namely transfer of the enol proton to the alcohol and transfer of the alcohol proton to the methylene group. We have found from model calculations that such a relay process is considerably slower than direct tunneling. Hence, the rate of this process in the stable complex will be considerably lower than that of hydrogen-bond dissociation.

In the metastable 2MAP-dMe complex, which is present in low concentration, the hydrogen bond destabilizes the **Z-II** configuration. Although it has a lower tunneling barrier, this barrier is still substantially higher than the barrier for splitting off the solvent molecule, thus favoring the latter process. The observation of a large KIE confirms that overbarrier proton transfer is not competitive for this complex either.

4 Discussion

Because of their wide temperature range, the measurements of GWT on 2MAP provide a unique set of data on a proton transfer reaction, showing curved Arrhenius plots along with a strong dependence of the KIE on temperature. However, these data have never found a satisfactory explanation. Although GWT, who noted the discrepancy between the isotope effect and the effective activation energies, correctly surmised that the reaction involved more

than one step, their identification of the additional step as a rotamer transition was not based on specific evidence. No further attempts have been reported to account for the observations. The present calculation corrects this situation by showing that the additional reaction step proposed by GWT must be discarded on energetic grounds: The suspected metastable enol rotamer turns out to be the stable one by a substantial margin. Tunneling calculations based on a direct dynamics method that includes all molecular vibrations lead to a model in which the enol–keto reaction occurs in two steps, namely dissociation of the enol-alcohol hydrogen bond followed by proton tunneling. The nonlinearity of the Arrhenius plot is well reproduced by the tunneling calculations. The contribution from the dissociation steps of the donor and acceptor complexes is small. The apparent absence of a direct tunneling contribution of the undissociated complexes is in line with observations made earlier [4] for phenolic compounds.

Our conclusion that the anomalous temperature dependence of this tunneling reaction is a solvent effect can be tested experimentally by carrying out the reaction in an aprotic solvent, if this can be found. Our prediction is that the reaction will then proceed much faster and show a much weaker temperature dependence, while the curvature of the Arrhenius plots and the isotope effect remain essentially unaltered.

Appendix: Summary of the AIM/DOIT approach

The instanton formalism is a multidimensional quasiclassical approach to tunneling rate phenomena based on the concept of least action. Here it is applied to a system where tunneling along the reaction coordinate x is coupled to vibrations $\mathbf{y}$, described by the Hamiltonian

$$H[x(\tau), \mathbf{y}(\tau)] = \frac{1}{2}\dot{x}^2 + \frac{1}{2}\dot{\mathbf{y}}^2 + U(x, \mathbf{y}). \tag{A.1}$$

The Euclidian action of this system (in imaginary time $\tau = it$; $\beta = 1/k_B T$)

$$S_{\mathrm{E}}(T) = \int_{-\beta\hbar/2}^{\beta\hbar/2} d\tau H[x(\tau), \mathbf{y}(\tau)] \tag{A.2}$$

has an extremum, defined by the equation $\delta S_{\mathrm{E}} = 0$. Two trivial solutions of this equation correspond to the (quasi)equilibrium configuration and the transition state (TS), the latter being a saddle point. Below a specific (crossover) temperature T_{ins}, there is another extremal trajectory, called the instanton (bounce) path, which is also a saddle point. The two saddle

points contribute to the imaginary part of the partition function, which in turn defines the rate constant of decay of the metastable configuration. The TS contributes a term proportional to e^{-U_0/k_BT}, where U_0 is the barrier height, and the instanton a term propotional to $e^{-S_{\rm I}(T)}$, where $S_{\rm I}$ is the Euclidian action (in units $\hbar$) corresponding to the instanton path. The rate constant at $T < T_{\rm ins}$ is thus of the form

$$k_{\rm tun}(T) = A(T)e^{-S_{\rm I}(T)}, \tag{A.3}$$

where the prefactor $A(T)$ represents the effect of trajectories adjacent to the instanton path. At $T \to T_{\rm ins}$ the instanton converges into the TS and the rate is that of an over-the-barrier transition. At $T > T_{\rm ins}$ the rate can thus be evaluated by standard methods, e.g. by transition-state theory

$$k_{\rm cl}(T) = \frac{k_BT}{h}\frac{Z^{\rm TS}}{Z^{\rm R}}e^{-U_0/k_BT}, \tag{A.4}$$

where $Z^{\rm TS}$ and $Z^{\rm R}$ are the partition functions of the TS and the reactant, respectively.

If many degrees of freedom affect the transfer, direct evaluation of the instanton trajectory is not feasible and therefore approximations are necessary. AIM is an approximation scheme for the evaluation of $S_{\rm I}(T)$ whereby direct search for the instanton trajectory is avoided. First, the multidimensional potential-energy surface is generated in a form suitable for the instanton calculations. It is derived from *ab initio* calculations of the structure, energy, and force field of the initial, final, and TS configuration, and formulated in terms of the normal modes of the TS which is taken as the origin. The mode x with imaginary frequency ω^* is the reaction coordinate and the remaining transverse modes $\mathbf{y}$ are treated as independent harmonic oscillators coupled linearly to x. Then the required coupling constants are derived from the displacements of the modes between the stable configurations and the TS. This coupling will enhance or suppress tunneling, depending on whether the coupled mode is symmetric (s) or antisymmetric (a) relative to reflection in the dividing plane $x = 0$. For systems with a symmetric double-well potential, the displaced modes are either (s) or (a), the reaction coordinate being of the latter type. For asymmetric systems, like the one at hand, the displacement of each mode can be separated into an (s) and (a) component. Antisymmetric coupling contributes effectively to the Franck-Condon factor of the transition (or friction) and thus lowers the rate. Symmetric coupling facilitates the transfer through

the lowering of the effective barrier height and width. The instanton action $S_{\rm I}(T)$ is obtained based on generalizations of known solution for low-dimensional models, in the form

$$S_{\rm I}(T) = \frac{S_{\rm I}^0(T)}{1+\sum_s \delta_s(T)} + \alpha \sum_a \delta_a(T), \tag{A.5}$$

and the preexponential factor $A(T)$ is approximated by

$$A(T) = \omega_0/2\pi, \tag{A.6}$$

ω_0 being the effective frequency of the reaction coordinate in the initial state. In Eq. (A.5) $S_{\rm I}^0(T)$ is the instanton action of 1D motion in the vibrationally-adiabatic potential (i.e. the adiabatic potential with zero-point corrections to the barrier height) and with renormalized mass $m_{\rm eff}(x)$. As seen from Fig. 2, the tunneling potential is strongly asymmetric and very steep at the point where the tunneling proton exits the barrier; it is therefore treated as an "absorbing wall". The action $S_{\rm I}^0(T)$ is evaluated as the "short" action, i.e. starting from the zero-point energy in the well, which in turn defines the preexponent in the form of Eq. (A.6). The renormalized mass comprises the effect of (a,s) modes that are "fast" on the time-scale $t^* \sim 1/|\omega^*|$ of motion under the barrier, and is of the general form $m_{\rm eff}(x) = 1+\Delta m_a+\Delta m_s x^2 \geq 1$ (in dimensionless units). Coupling to the "slow" (a,s) modes contributes via the corrections $\delta_{a,s}(T)$ and the factor $\alpha < 1$ describes the modulation of the Franck-Condon factor by the (s) modes. The effective parameters ω_0 and $m_{\rm eff}(x)$ and the corrections $\delta_{a,s}(T)$ are expressed analytically in terms of the normal mode frequencies and displacements, and the evaluation of $S_{\rm I}^0(T)$ for a given temperature is performed through a simple numerical integration. The temperature dependence of $S_{\rm I}^0(T)$ is weak, since it corresponds to thermal excitation of the motion of the high-frequency O-H vibration. The main temperature dependence of the tunneling rate in Eq. (A.3) with the action from Eq. (A.5) is thus due to the terms $\delta_{a,s}(T)$, as it is related to thermal excitation of relatively low-frequency modes. The crossover temperature is of the order $T_{\rm ins} \sim |\omega^*|/2\pi$, which means that for practical implementation one needs a smooth link between the low-temperature range of deep tunneling and the high-temperature range of pure classical transfer. In AIM/DOIT1.2 such link is provided by representing the overall rate constant in the form

$$k(T) = k_{\rm tun}(T) + k_{\rm cl}(T), \tag{A.7}$$

which is the expression used in the main text for the rate constant of the **Z-II**–keto transformation.

The input parameters for the DOIT1.2 code are standard electronic-structure data and Hessians of the three stationary configurations: reactant, TS and product. The adiabatic potential, illustrated in Fig. 2, was calculated as projection onto x of the potential along the minimum energy path. In the present study the data were obtained at the MPWB1K/6-31+G(d,p) level of theory; the main parameters are summarized in Table 1. The main parameters of the AIM/DOIT1.2 calculations are summarized in Table 2. More detail on the AIM/DOIT1.2 procedure in application to proton transfer in asymmetric potentials can be found in refs. [5,8,9].

References

[1] W. Siebrand and Z. Smedarchina, J. Phys. Chem. B 115 (2011) 7679.

[2] J.C. Scaiano, Chem. Phys. Lett. 73 (1980) 319.

[3] K.-H. Grellmann, Weller, H. and E. Tauer, Chem. Phys. Lett. 95 (1983) 195.

[4] L. Valglimigli, J.T. Banks, K.U. Ingold and J. Lusztyk, J. Am. Chem. Soc. 117 (1995) 9966.

[5] W. Siebrand, Z. Smedarchina, M.Z. Zgierski, A. Fernández-Ramos, Int. Rev. Phys. Chem. 18 (1999) 5; Z. Smedarchina, A. Fernández-Ramos, and W. Siebrand, J. Comp. Chem. 22 (2001) 787.

[6] Y. Zhao, D. G. Truhlar, J. Phys. Chem. A 108 (2004) 6908.

[7] Gaussian 03, Revision B.05, M. J. Frisch, G. W. Trucks, H. B. Schlegel, G. E. Scuseria, M. A. Robb, J. R. Cheeseman, J. A. Montgomery, Jr., T. Vreven, K. N. Kudin, J. C. Burant, J. M. Millam, S. S. Iyengar, J. Tomasi, V. Barone, B. Mennucci, M. Cossi, G. Scalmani, N. Rega, G. A. Petersson, H. Nakatsuji, M. Hada, M. Ehara, K. Toyota, R. Fukuda, J. Hasegawa, M. Ishida, T. Nakajima, Y. Honda, O. Kitao, H. Nakai, M. Klene, X. Li, J. E. Knox, H. P. Hratchian, J. B. Cross, V. Bakken, C. Adamo, J. Jaramillo, R. Gomperts, R. E. Stratmann, O. Yazyev, A. J. Austin, R. Cammi, C. Pomelli, J. W. Ochterski, P. Y. Ayala, K. Morokuma, G. A. Voth, P. Salvador, J. J. Dannenberg, V. G. Zakrzewski, S. Dapprich, A. D. Daniels, M. C. Strain, O. Farkas, D. K. Malick, A. D. Rabuck, K. Raghavachari, J. B. Foresman, J. V. Ortiz, Q. Cui, A. G. Baboul, S. Clifford, J. Cioslowski, B. B. Stefanov, G. Liu, A. Liashenko, P. Piskorz, I. Komaromi, R. L. Martin, D. J. Fox, T. Keith, M. A. Al-Laham, C. Y. Peng, A. Nanayakkara, M. Challacombe, P. M. W. Gill, B. Johnson, W. Chen, M. W. Wong, C. Gonzalez, and J. A. Pople, Gaussian, Inc., Wallingford CT, 2004.

[8] Z. Smedarchina, W. Siebrand, A. Fernández-Ramos, L. Gorb, and J. Leszczynski, J. Chem. Phys. 112 (2000) 566.

[9] A. Fernández-Ramos, Z. Smedarchina, and M.Z. Zgierski, J. Chem. Phys. 113 (2000) 2662.

Table 1: Calculated relative energies (in kcal/mol) of the equilibrium configurations and (rotational and tunneling) transition states of 2MAP and two 1:1 complexes with (proton-donor and -acceptor) methanol molecules. $\Delta E_{\mathrm{I,II}}$ represents the hydrogen bond energy.

Molecule	**Z-I**	**Z-II**	keto	TS(rot)	TS(tun)	ΔE_{I}	ΔE_{II}
2MAP	3.89	0	-36.64	8.25	7.28	-	-
2MAP-dMe	-0.57	0	-38.93	4.15	6.47	4.91	4.34
2MAP-aMe	0	-0.98	-38.93	5.69	9.27	4.91	5.89

Table 2: Main parameters of AIM/DOIT1.2 related to the evaluation of the rate constant $k_2(T)$ of proton-transfer between **Z-II** and the keto form (see Appendix).

Parameter	2MAP	2MAP-d_1
Vibrationally-adiabatic barrier height	7.92 kcal/mol	7.85 kcal/mol
Displacement Donor-TS	0.692 Å.amu$^{1/2}$	0.870 Å.amu$^{1/2}$
Displacement TS-Acceptor	1.014 Å.amu$^{1/2}$	1.393 Å.amu$^{1/2}$
Effective frequency of the reactant well	2484.8 cm^{-1}	1806.1 cm^{-1}
Effective frequency of the product well	1475.9 cm^{-1}	1133.0 cm^{-1}
Imaginary frequency $\|\omega^\star\|$	1403.7 cm^{-1}	1073.3 cm^{-1}
1D action $S^0_{1\mathrm{D}}(T=0/T=300K)$	8.782/7.786	14.895/10.308
Parameter of enhancing coupling $\sum_s \delta_s(T=0/T=300K)$	0.251/0.347	0.208/0.340
Parameter of suppressing coupling $\alpha \sum_a \delta_a(T=0/T=300K)$	9.933/3.603	9.934/3.522
Effective mass of tunneling $m_{\mathrm{eff}}(x)$	1.12+3.63x^2	1.16+3.71x^2
$k_{2,\mathrm{tun}}(T=0\ K)$	3.23.10^6 s^{-1}	1.16.10^4 s^{-1}
$k_{2,\mathrm{tun}}(T=300\ K)$	7.70.10^9 s^{-1}	9.86.10^8 s^{-1}
$k_{2,\mathrm{cl}}(T=300\ K)$	1.30.10^9 s^{-1}	2.55.10^8 s^{-1}

Figure captions

1. Structures of the keto, the two **Z**-enol forms and two transition states (between **Z-I**−**Z-II** and between **Z-II**−keto) of 2MAP. Some distances (in Å) associated to the proton transfer are indicated.

2. The adiabatic potential for the **Z-II**−keto transition used in the AIM/DOIT calculations, shown as a function of the reaction coordinate, which is the mode with imaginary frequency at the transition-state configuration in our approach. The potential is scaled by the barrier height listed in Table 1 and the coordinate is scaled by the displacement between the donor and the transition-state configuration listed in Table 2. The solid/broken lines correspond to H/D transfer.

3. Arrhenius plot of the **Z-II**−keto transition rate constants $k^{\mathrm{H,D}}(T)$. The two thick solid lines in the center are the calculated results from Eq. (1) and the solid and open circles are the experimental results for 2MAP and 2MAP-d_1, respectively, as reported by GWT [3]. The two thin lines at the top represent the calculated proton and deuteron rate constants $k_2^{\mathrm{H}}(T)$ and $k_2^{\mathrm{D}}(T)$. The broken line at the bottom represents the statistical factor to $k_2(T)$, given by Eq. (1). The two thick dot-dashed lines represent the rates from the exponential fit $k(T) = k_2(T)\exp(-5.55/k_BT)$.

4. Structures of the two **Z-II**-methanol complexes in the equilibrium configuration and in the **Z-II**−keto transition state: (a) the hydrogen-donor complex and (b) the hydrogen-acceptor complex. Some distances (in Å) associated to the proton transfer are indicated.

Figure1

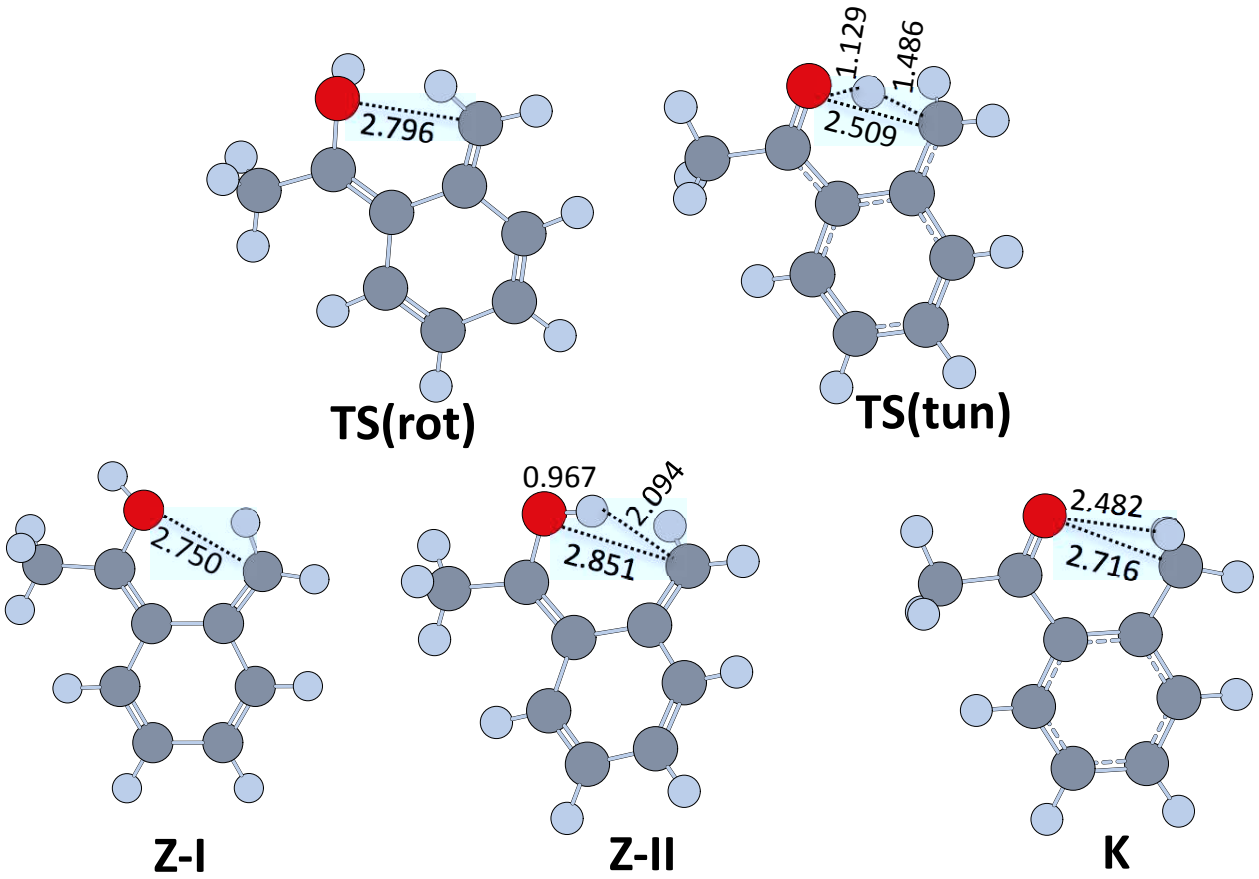

Figure 1

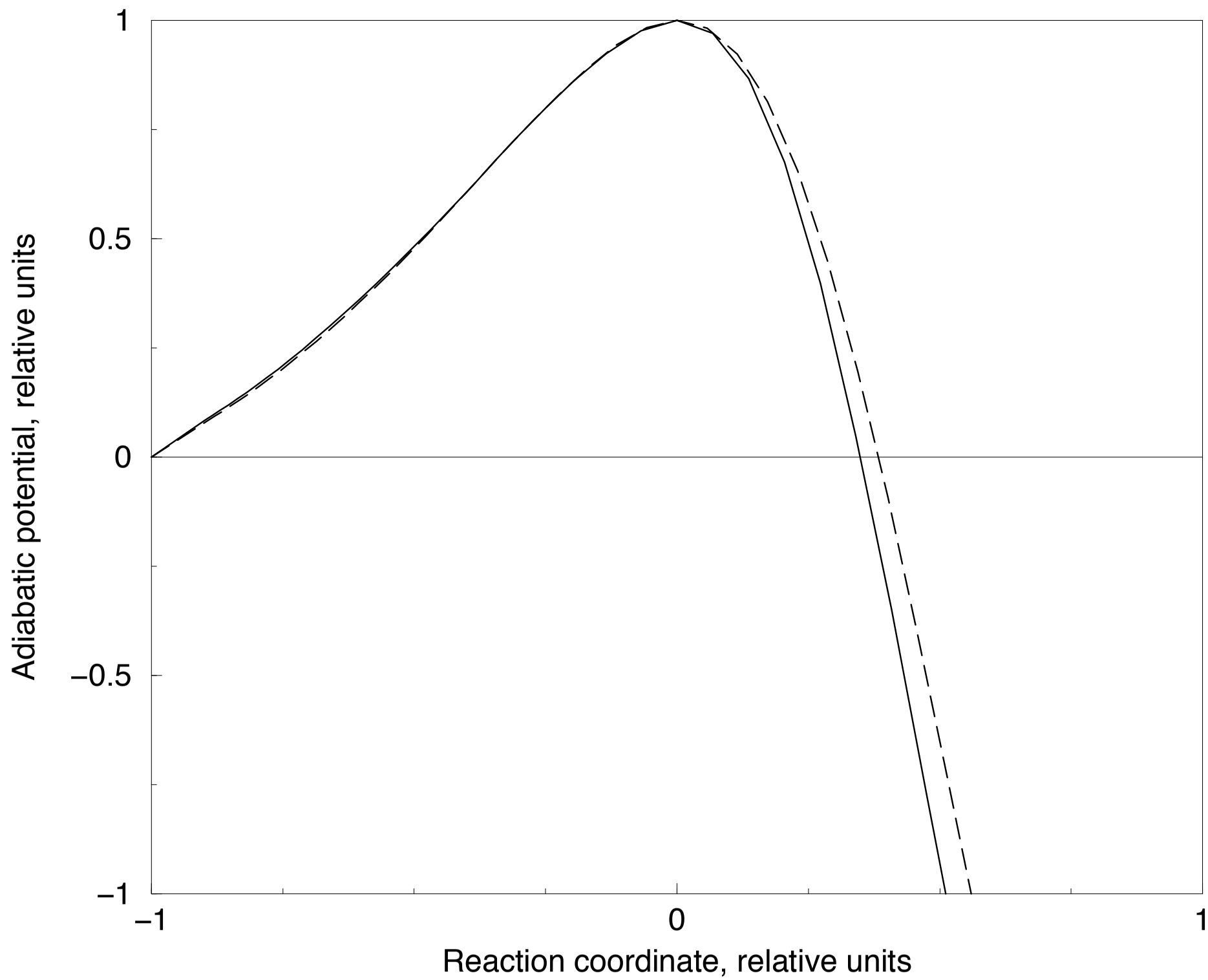

Figure2

Fig. 2

Figure3

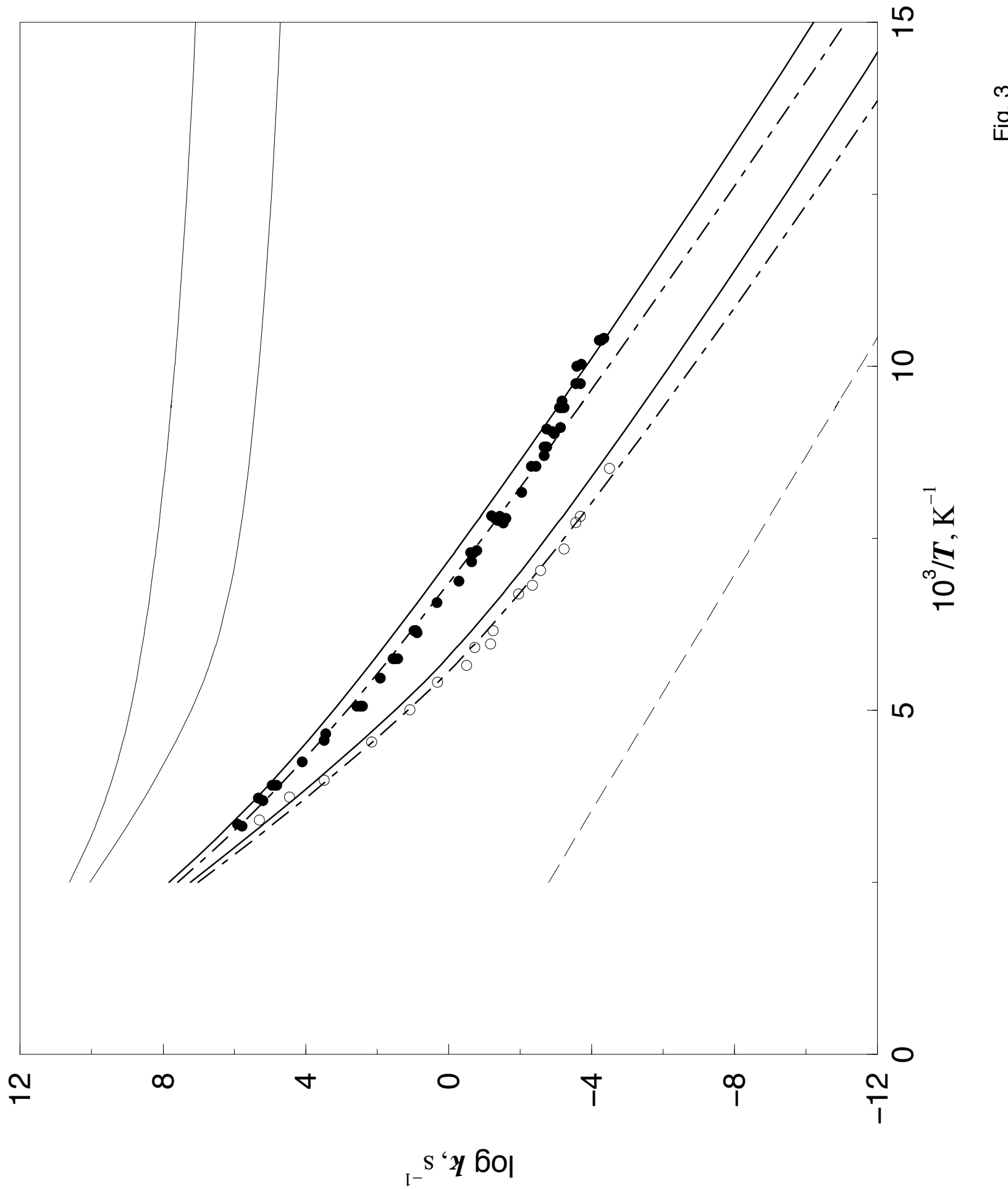

Fig. 3

Figure4

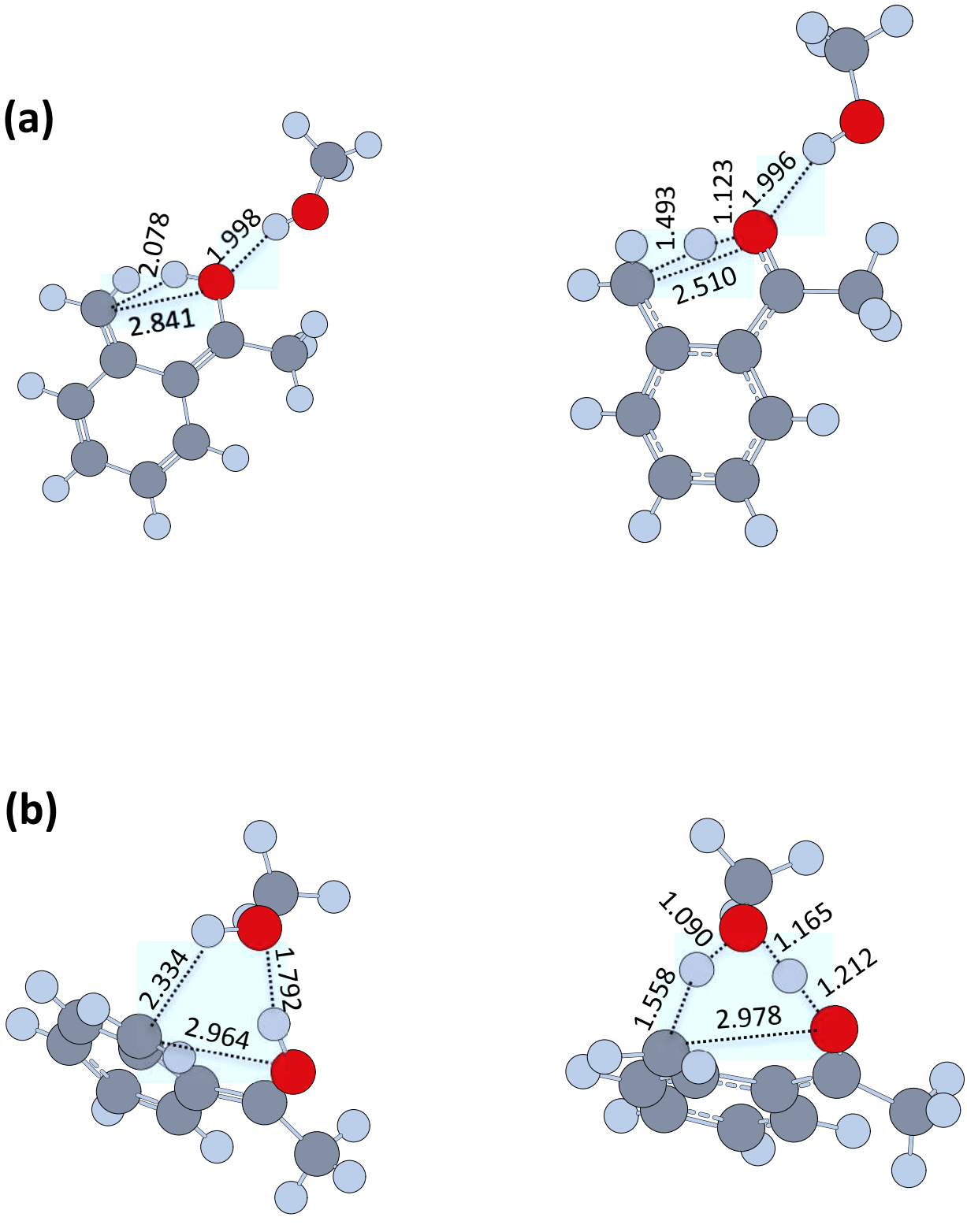
(a)
2.078
1.998
2.841
1.493
1.123
1.996
2.510
(b)
2.334
1.792
2.964
1.090
1.165
1.212
1.558
2.978